SCIENTIFIC REPORTS

OPEN

SUBJECT AREAS:
NANOCOMPOSITES
BATTERIES

Received
25 November 2013

Accepted
21 January 2014

Published
6 February 2014

Correspondence and requests for materials should be addressed to X.F.L. (lixianfeng@dicp.ac.cn) or H.M.Z. (zhanghm@dicp.ac.cn)

Membranes with well-defined ions transport channels fabricated via solvent-responsive layer-by-layer assembly method for vanadium flow battery

Wanxing Xu[1,2], Xianfeng Li[1], Jingyu Cao[1,2], Hongzhang Zhang[1] & Huamin Zhang[1]

[1]Division of energy storage, Dalian Institute of Chemical Physics, Chinese Academy of Sciences, Zhongshan Road 457, Dalian 116023, China, [2]University of Chinese Academy of Sciences, Beijing 100039, China.

In this work we presented a general strategy for the fabrication of membranes with well-defined ions transport channels through solvent-responsive layer-by-layer assembly (SR-LBL). Multilayered poly (diallyldimethylammonium chloride) (PDDA) and poly (acrylic acid) (PAA) complexes were first introduced on the inner pore wall and the surface of sulfonated poly (ether ether ketone)/poly (ether sulfone) (PES/SPEEK) nanofiltration membranes to form ions transport channels with tuned radius. This type of membranes are highly efficient for the separators of batteries especially vanadium flow batteries (VFBs): the VFBs assembled with prepared membranes exhibit an outstanding performance in a wide current density range, which is much higher than that assembled with commercial Nafion 115 membranes. This idea could inspire the development of membranes for other flow battery systems, as well as create further progress in similar areas such as fuel cells, electro-dialysis, chlor-alkali cells, water electrolysis and so on.

Large-scale energy storage has attracted increasing interests due to its urgent need in grid management (load leveling and peak shaving), the grid reliability and utilization and the integration of renewable energy sources[1–3]. Among a wide range of energy storage technologies, vanadium flow battery (VFB) has a unique combination of high efficiency, high reliability, flexible design and long cycle life, which makes it an ideal candidate for large scale energy storage[4–6]. VFB, originally proposed by Maria Skyllas-Kazacos in 1985, consists of two electrolyte tanks with active species of vanadium ions in different valance states, two pumps and a battery cell[7]. A separator alternatively called membrane, as one of the key components of a VFB cell, is employed to prevent the cross mixing of the positive and negative electrolytes and complete the current circuit by transferring ions[8]. Currently, urgent needs are still in the fabrication of membrane separators for these batteries under the recognition that high-quality membranes with low cost are vital to achieve large-scale acceptable VFB systems[9]. Among these membranes, ions transport properties are the key factors in determining their final performance.

Ions transport across membrane mainly depends on the unique features of nanoscale ions transport channels, e.g. the geometry and surface charge characteristics[10,11]. When channel dimensions are on the order of the Debye length, the surface characteristic of the channels plays a significant role in the ionic behavior[12]. Hence, to fabricate membranes with well-defined nanoscale ions transport channels via tuning its size and the surface characteristics is crucial to understand its structure-morphology-property relationships and ions transport mechanism.

The layer-by-layer (LBL) assembly technique provides a versatile means to create polymeric thin films, allowing nanometer-scale control over the spatial distribution of ionized species within the membrane[13–16]. The principle of the LBL assembly technique is based on the alternate adsorption of oppositely charged species on the surface of substrates via electrostatic or hydrogen-bonding interactions[17]. Considerable efforts have been made to extend this technique to various materials such as porous membranes[18,19], light emitting polymers[20], biopolymers and various inorganic particles[21–23]. Considering the excellent hydrophilicity of polyelectrolyte (PE)[24], it could be possible to fabricate membranes with well-defined ions transport channels through introducing the PE layers on the inner pore wall and the surface of porous template membranes (Fig. 1a). However, the pore

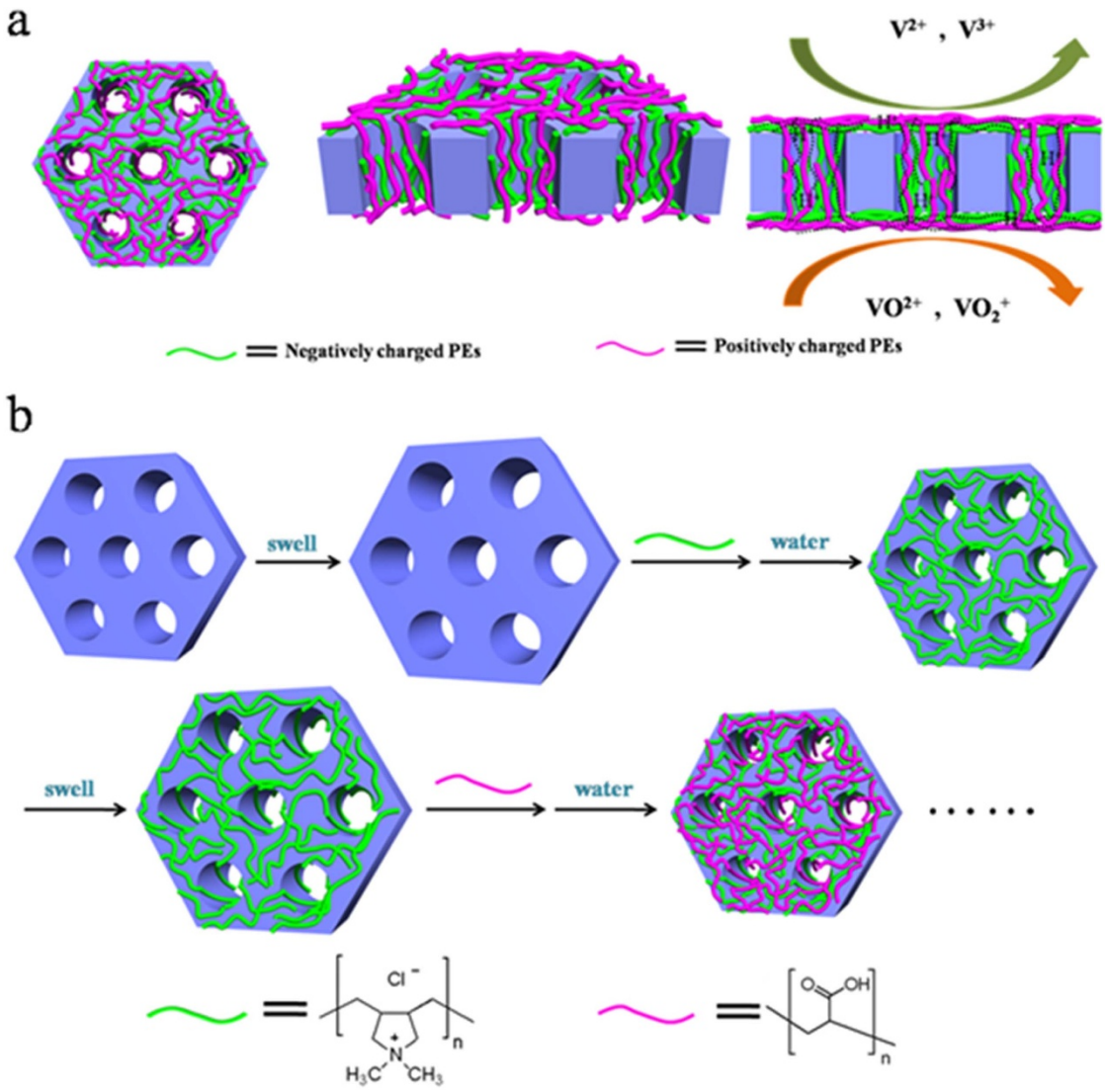

Figure 1 | (a) Schematic principle of membranes with well-defined ions transport channels. (b) Schematic of the solvent-responsive layer-by-layer assembly process.

size of the template membranes should be in the range of nanoscale to create ions transport channels with a proper controlled window of channel radius. Nanofiltration (NF) is a pressure driven membrane process involving pressures between 5 and 20 bars. The normal pore size of NF membranes is in the range of nanometers, thereby is suitable as porous template. Therefore, to introduce multilayered PEs in NF membranes could create "ions transport channels" with controlled size and electrostatic nature via adjusting the number and composition of PE layers. Compared to the membranes prepared by the conventional LBL method, these structures could effectively improve the ions conductivity of membrane on the basis of excellent ions selectivity. However, it is difficult to deposit PE layers through LBL method on the inner pore wall of NF membrane because of its too small pore size[25]. It is therefore of vital importance to tune the "open or close" state of pore structure of NF membrane to introduce the PE layers into its inner pore wall.

Considering the different affinity between the polymer and solvent, the solvent can get into the polymer membrane to bring about different solubility when treating this membrane with different solvents[26]. In the view of thermodynamics, this process could allow small molecules to get into the polymer networks thus increase the distance between the polymer chains and weaken their twine to enhance their mobility, which leads to the change in free volume of these networks[27]. When numerous small molecular solvent gets into the inner structure of membrane, the polymer will come about the swelling or dissolving. Thus, it could tune the free volume of the polymer membrane via treating the membranes with proper solvent, here, we called solvent-responsive, therefore realizing the control of "open" or "close" state of the membrane pores.

In this paper, we firstly introduce solvent-responsive layer-by-layer assembly (SR-LBL), which combines the well-known LBL assembly with solvation interactions, to fabricate membranes with defined ions transport channels. The ions transport channels of membranes are fabricated by depositing PE layers on the inner pore wall as well as the surface of polymer membranes after swelling in the solvent. It is expected that membranes fabricated by this method could exhibit excellent ions selectivity, because of the dramatically decreased pore size of membranes, while maintaining high ions conductivity, due to the improvement in hydrophilicity for membranes. The structure of membranes is characterized by field emission scanning electronic microscopy (FE-SEM), energy-dispersive X-ray spectroscopy (EDS), transmission electronic microscopy (TEM) and atomic force microscopy (AFM). These results are correlated with the solubility parameters[28–30] to elucidate further the effect of swelling behavior on the ions transport performance of membranes. In particular, the VFB performance of solvent-responsive multilayered

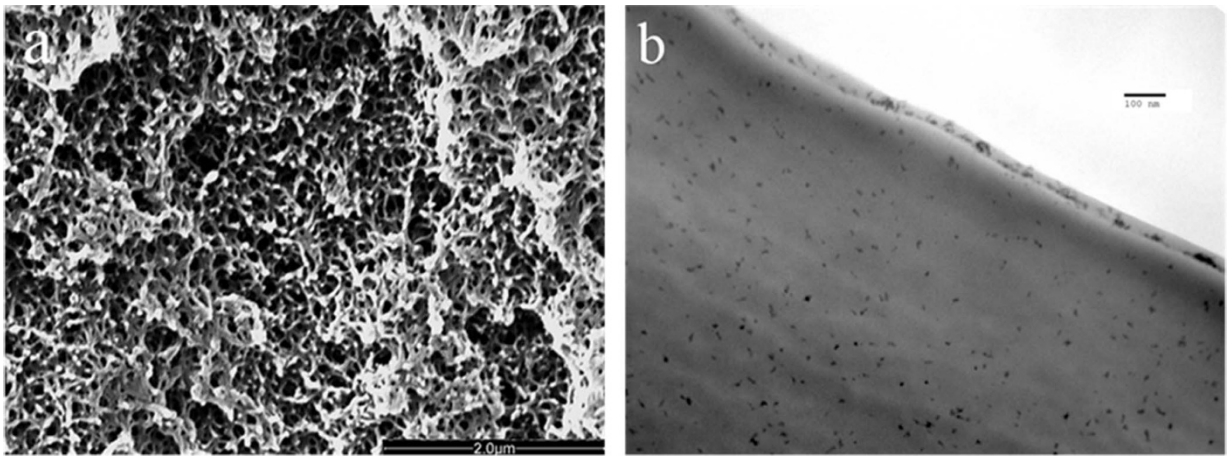

Figure 2 | **Cross-section morphology (a) and distribution of charged groups (b) of prepared substrate membrane.**

membranes and their chemical stability are investigated. These results enable us to gain a deep understanding of the swelling behavior of membranes and provide a general method to fabricate membranes with well-defined ions transport channels.

Results

Cross-section morphology characterization of substrate membrane. To fabricate porous substrate with fixed charges for SR-LBL assembly, the negatively charged PES/SPEEK NF membranes were fabricated via a typical phase inversion method. Substrate membranes were prepared from a solution containing 28 wt% PES and 7 wt% SPEEK in N,N-Dimethylacetamide and cast with a wet thickness of around 130 μm. The cross-section morphology of substrate membrane was characterized with FE-SEM and TEM. The cross-section morphology of substrate membrane in Fig. 2a clearly shows a spongy structure. TEM was performed on the cross-section of substrate membrane after staining with $[Pb(Ac)_2]^{2+}$ to further investigate the distribution of negatively charged sulfonic groups from SPEEK. The dark spots of substrate membrane in Fig. 2b are ascribed to clusters formed by the interaction between $[Pb(Ac)_2]^{2+}$ and negatively charged sulfonic groups of SPEEK, showing the uniform distribution of charged SPEEK in the inner structure and enrichment on the surface.

Swelling of the dry substrate membrane in different solvents. As seen in Fig. 3, a sequence for the swelling of the dry substrate membrane is in the order of isopropanol (IPA) > methanol > ethylene glycol (EG) > water. In this paper, methanol was firstly selected as swelling agent to treat the charged PES/SPEEK substrate membrane due to the fact that PDDA cannot be dissolved in IPA. 3, 5 and 7 layers of PAA/PDDA were introduced in the pores and on the surface of substrate membranes to form ions transport channels.

EDS and TEM analysis. The EDS and TEM measurements were carried out to confirm the channel structures. The nitrogen element content of membranes cross-section was initially detected by EDS to investigate the channel structures, since the characteristic element for PDDA/PAA multilayered membranes is nitrogen from PDDA. The weight percent of nitrogen element of membranes is summarized in Fig. 4a. The weight percent of nitrogen element of substrate membrane was zero, while the weight percent of nitrogen element of methanol-responsive multilayered membranes increased from 0.92% to 1.52% with the increasing PE layers, which confirms that the PE layers have been successfully introduced into the inner pore structure of membranes. To provide a better understanding of the PDDA/PAA multilayer distribution in the cross-section of membranes, methanol-responsive multilayered membranes were characterized using both TEM and EDS. TEM was performed on the cross-section of membranes after staining with $[Pb(Ac)_2]^{2+}$ to further investigate the distribution of negatively charged SPEEK and PAA (Fig. 4b). Compared with the initial PES/SPEEK porous substrate, the dark sports formed by interactions between $[Pb(Ac)_2]^{2+}$ and negatively charged sulfonic groups in membrane cross-sections disappeared after assembling multilayered PE in membranes pores. This is because the formed PDDA/PAA multilayer in the inner structure significantly lowered the net amount of the negatively charge density. Moreover, a top layer with a thickness of about 300 nm was clearly illustrated on the membrane surface. EDS map for methanol-responsive membrane with 5 PE layers further confirmed the existence of PDDA in the inner pore structure of methanol-responsive multilayered membranes (Fig. 4c and 4d).

ATR-FTIR and SEM analysis. Similar to the well-known LBL assembly method, the newly introduced SR-LBL assembly method also introduces the PDDA/PAA multilayers on the surface of membranes except that it favors the deposition of the PDDA/PAA

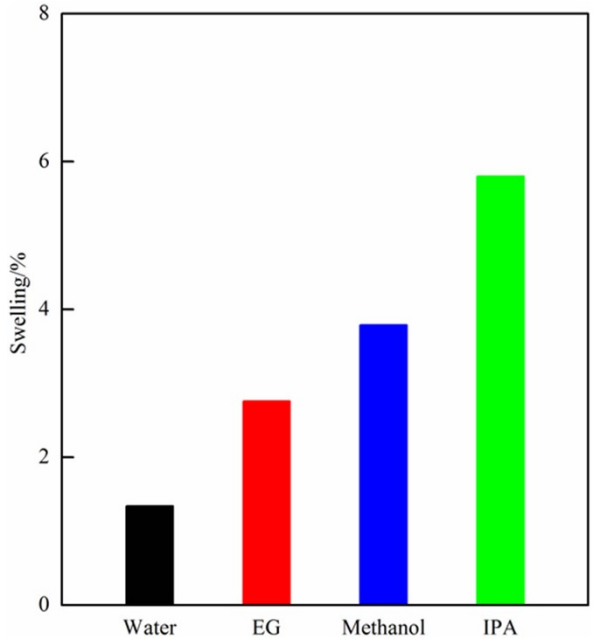

Figure 3 | **Swelling of the dry substrate membrane in water, EG, Methanol and IPA.**

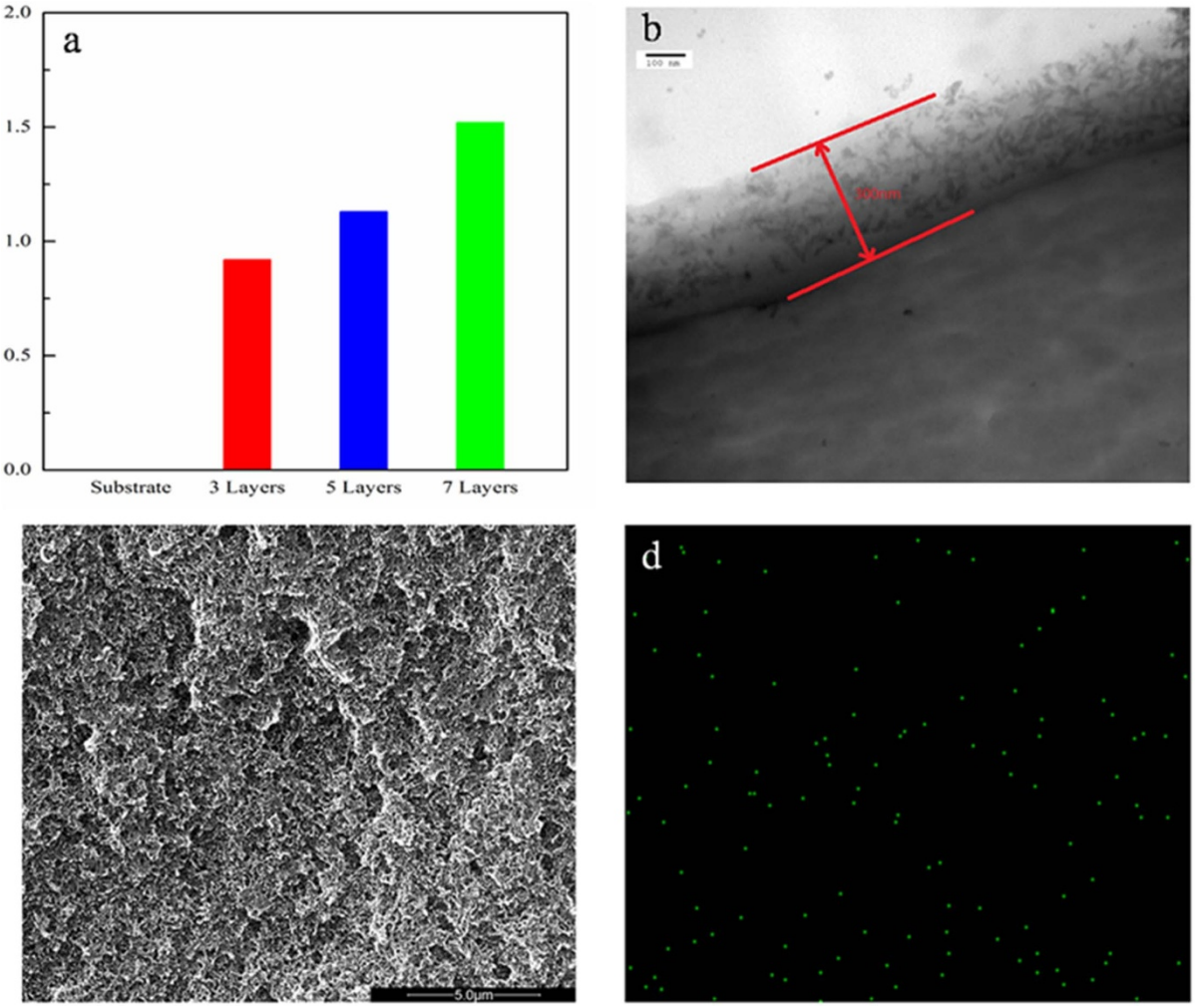

Figure 4 | (a) Weight percent of nitrogen element of substrate membrane and methanol-responsive multilayered membranes. (b) TEM image of methanol-responsive membrane with 5 PE layers. (c) FE-SEM cross-section image of methanol-responsive membrane with 5 PE layers used for (d) EDS mapping of N distribution, confirming the presence of PDDA in the inner pore structure.

multilayers in the inner pores. In order to investigate the impact of the PDDA/PAA multilayers on the surface structure of membranes, the ATR-FTIR spectra were performed on substrate membrane and methanol-responsive multilayered membranes. The results were displayed in Fig. 5. Peaks at 2920 cm^{-1} and 2850 cm^{-1} are attributed to asymmetrical CH_2 and symmetrical CH_2 stretching of PDDA. The stretching peaks at 1750 cm^{-1} are attributed to the C=O groups of PAA. The peaks clearly increase along with increasing PE layer number, confirming the existence of PDDA and PAA into the membrane structure. In addition, SEM was used as a supplemental technique to gain insight into the effect of the deposition of PDDA/PAA multilayers on the surface structure of membranes. The surface morphologies reported in Supplementary Fig. S1 show that the substrate membrane exhibits a smooth surface, while the surface of methanol-responsive multilayered membranes exhibit a increased roughness along with increasing number of PE layers. AFM was carried out to further investigate the surface roughness of the prepared membranes. The images given in Supplementary Fig. S2 show that the average roughness of the membranes (*Ra*) increases from 6.854 nm to 8.888 nm after introducing 3 PE layers on the surface of the substrate membrane. Accordingly their surface porosity should increase as well with increasing the PE layer numbers, which possibly is beneficial to increase ions conductivity. These results indicate that PDDA/PAA multilayers have been successfully introduced on the surface of membranes, which is

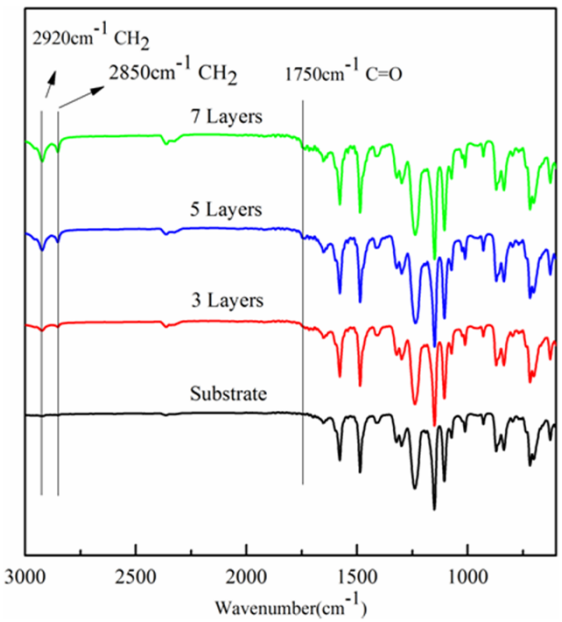

Figure 5 | **ATR-FTIR spectra of substrate membrane and methanol-responsive multilayered membranes.**

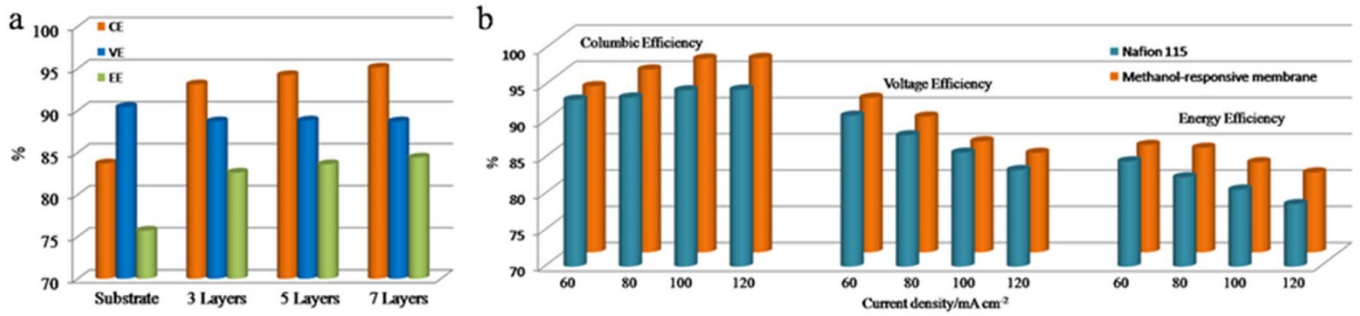

Figure 6 | (a) VFB performance of methanol-responsive membranes with different PE layers. (b) VFB performance of methanol-responsive membrane with 7 PE layers vs. Nafion 115 under different current densities.

consistent with those reported in the literature for multilayered PE complex based membranes[31].

Battery performance. We further study VFB performance of methanol-responsive multilayered membranes. Firstly, the methanol-responsive membranes with different PE layers were tested on the VFB as reported in Fig. 6a. The columbic efficiency (CE), which is defined as the ratio of a cell's discharge capacity divided by its charge capacity, increases dramatically from 83.7% to 95.1% along with the PE layers range from 0 PE layers to 7 PE layers. The voltage efficiency (VE), which is determined by the ratio of a cell's mean discharge voltage to its mean charge voltage, decreases a little along with the PE layer. Thus the energy efficiency (EE), which is one of the most important parameters, increases dramatically from 75.7% to 84.4% with increasing the PE layer. In this system, the overall VFB performance of methanol-responsive multilayered membranes is much better than that of the substrate membrane.

The performance of VFB single cell assembled with methanol-responsive membrane with 7 layers of PEs under various current densities was also investigated. The result from Fig. 6b shows that the CE increases from 92.9% to 96.8% along with the current density increasing from 60 mA cm^{-2} to 120 mA cm^{-2}. This tendency is due to the less time required to finish a charge/discharge cycle at high current densities[32]. However, lower VE is observed with the increasing current densities due to the high overpotential and ohmic resistance at high current density[33]. In this system, much higher CE and EE than Nafion 115 were realized under comparable operating conditions with current densities range from 60 mA cm^{-2} to 120 mA cm^{-2}. This membrane exhibits EE of 81% at a current density of 120 mA cm^{-2}, which is much higher than that of commercial Nafion 115 membranes (EE 78.6%), confirming that membranes with well-defined ions transport channels and further well tuned VFB performance could be realized via SR-LBL assembly method.

To investigate the chemical stability of the membrane with ions transport channels under the practical conditions, the charge/discharge cycle test at a current density of 120 mA cm^{-2} was performed on the VFB assembled with methanol-responsive membrane with 7 PE layers (Figure 7a). The single VFB cell showed stable performance after running for more than 100 cycles. The CE remained around 96%, suggesting a low permeation rate of vanadium ions across membrane. The VE remained around 83%, indicating the membrane provided stable ions transport channels. In addition, SEM was performed on the membranes before and after the cycling test. Similar surface and cross-section morphologies shown in Fig. 7(b)–7(e) were found after the cycling test, confirming the excellent stability of the membranes with ions transport channels under the practical VFB conditions.

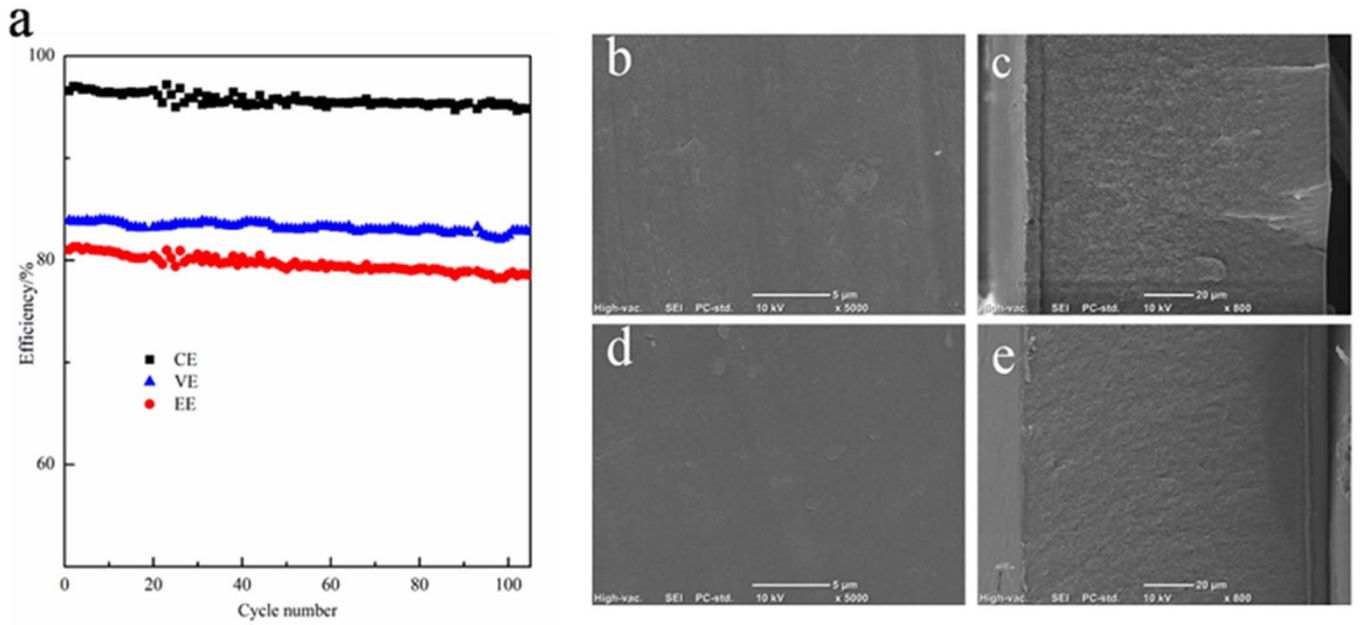

Figure 7 | (a) Cycling performance of VFB assembled with methanol-responsive membrane with 7 PE layers at a current density of 120 mA cm^{-2}. SEM image of methanol-responsive membrane with 7 PE layers: (b) initial surface morphology; (c) initial cross-section morphology; (d) surface morphology after the cycling test; (e) cross-section morphology after the cycling test.

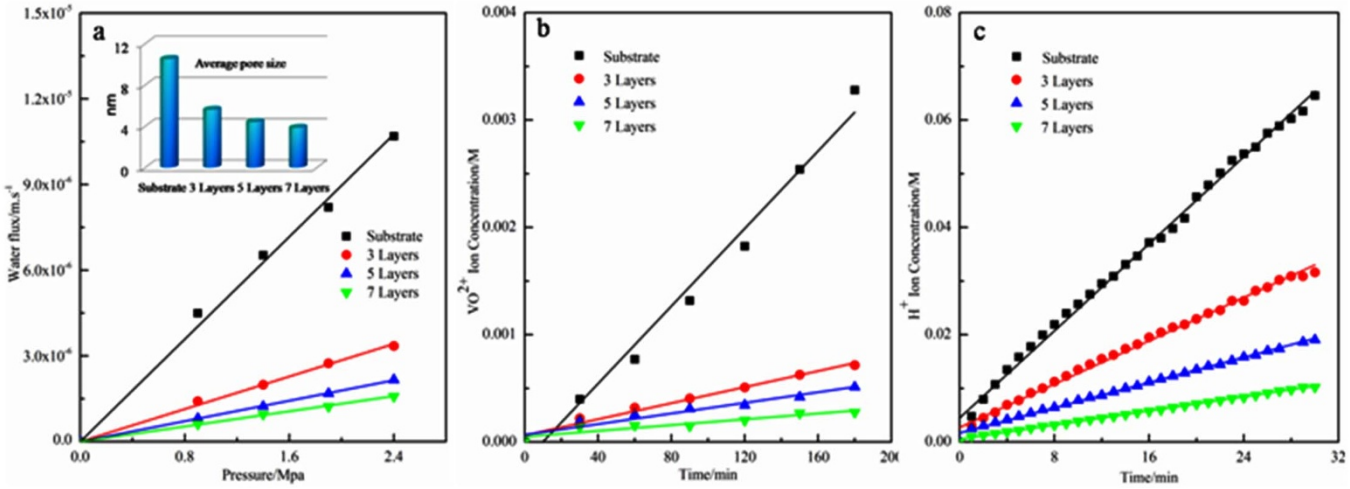

Figure 8 | (a) Water flux at different pressure and their average pore size of substrate membrane and methanol-responsive multilayered membranes. (b) VO^{2+} and (c) H^+ concentrations in the deficiency side of the diffusion cell with substrate membrane and methanol-responsive multilayered membranes.

Discussion

As one of the key factors to fabricate membranes with well-defined ions transport channels, solvent plays a significant role in adjusting the free volume or pore size of polymer membrane. Figure 1b provides the principle of the SR-LBL process. Unlike the traditional LBL method, solvent was applied in our present study to swell the membrane for some time to open the pores and allow PE having enough space to be deposited. The trend of the swelling of the dry substrate membrane shown above can be explained by the difference in the solubility between polymers and solvents. The solubility parameter as defined by Hansen, who took into account the dispersive forces, the polar interactions and hydrogen bond, is also called the Hansen solubility parameter (HSP)[28]. The total solubility parameter is defined as[26]:

$$\delta = \sqrt{(\delta_d^2 + \delta_p^2 + \delta_h^2)} \quad (1)$$

Where δ_d, δ_p, and δ_h are dispersive, polar, and hydrogen bonding solubility parameters, respectively. Solubility properties can be expressed using HSP with a three-dimensional coordinate system with axes δ_d, δ_p, and δ_h. The HSP coordinate of the solute is at the center of a sphere and the radius of the sphere, R_o, shows the maximum difference in affinity tolerable for complete solution to take place[28]. The relative energy difference (RED) has been defined according to equation (2) and (3)[28]:

$$(R_a)^2 = 4(\delta_{d1} - \delta_{d2})^2 + (\delta_{p1} - \delta_{p2})^2 + (\delta_{h1} - \delta_{h2})^2 \quad (2)$$

$$\mathrm{RED} = R_a / R_0 \quad (3)$$

The subscripts of 1 and 2 are for the solute and solvent, respectively. When RED $<$ 1, the corresponding solvent can dissolve the polymer, whereas when RED $>$ 1, the corresponding solvent cannot dissolve the polymer. Poorer solvents will have higher RED value. The HSP and R_o for PES are δ_d = 19.6, δ_p = 10.8, δ_h = 9.2 and R_o = 6.2, respectively[26]. The HSP for solvents are obtained from the published work[34]. As listed in Supplementary Table S1, the sequence for RED for PES in different solvents is in the order of IPA $<$ methanol $<$ EG $<$ water. Accordingly, the solubility of PES in the above four solvents is in the order of IPA $>$ methanol $>$ EG $>$ water, which is consistent with the sequence of the swelling of dry substrate membrane above.

To confirm that the pore size or the radius of ions transport channels could be tuned via changing the number of the deposited PE layers[35], the average pore size of polymer membranes was investigated via water permeability method. Fig. 8a shows the average pore size of substrate membrane and methanol-responsive multilayered membranes. It can be seen that the average pore size of membranes decreased as the number of deposited PE layers increased, which confirms the decreased pore size due to the deposition of PE layers on the inner pore wall of polymer membranes. As a result, the decreased average pore size of methanol-responsive membranes further lower their cross-mixing of vanadium ions and a higher CE can be obtained. Thus, membranes with well-defined "ions transport channels" could be realized via SR-LBL method. To further link ions transport channels structure of membranes with their selectivity, the permeability of VO^{2+} and H^+ across the membranes was detected as shown in Fig. 8b and 8c. The linear of VO^{2+}/H^+ concentration vs. time reflected the permeability of VO^{2+} and H^+ across membranes

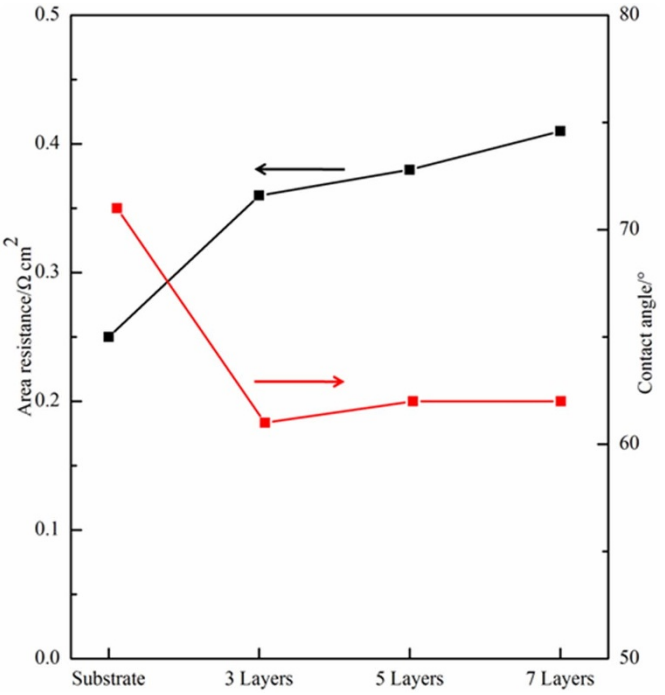

Figure 9 | **Area resistance and contact angle of substrate membrane and methanol-responsive multilayered membranes.**

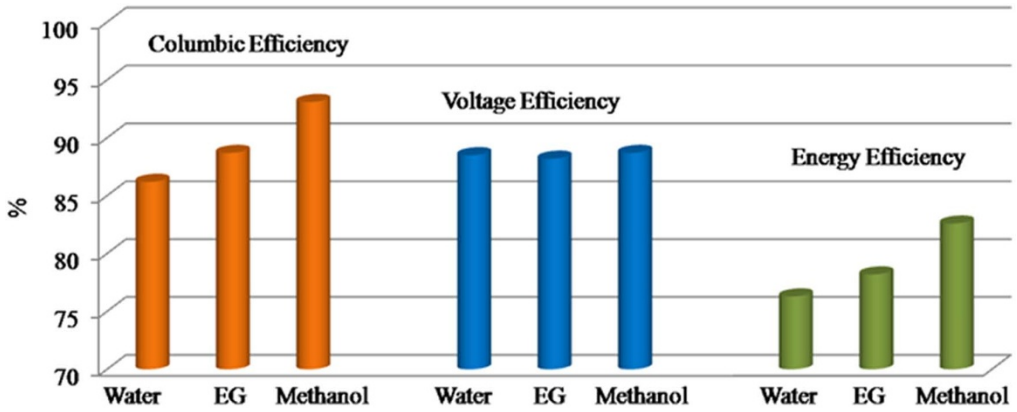

Figure 10 | VFB performance of methanol-responsive, EG-responsive and water-responsive membranes with 3 PE layers.

with various PE layers. As expected, the slope of the line decreases with the increasing PE layer, indicating the decreased pore size with the increasing PE layer. Compared with vanadium ions, protons transport much faster for all the membranes, since the Stokes radius of vanadium ions is much larger than that of protons[36,37].

The effect of the PE layers on the proton conductivity of membranes was conducted via the area resistance measurement displayed in Fig. 9. As expected, the area resistances of methanol-responsive membranes is slightly higher than that of substrate membrane due to the decreased pore size of methanol-responsive multilayered membranes, while the area resistance of methanol-responsive multilayered membranes was nearly unchanged with the increasing PE layers. The nearly unchanged area resistance of methanol-responsive multilayered membranes can be explained by the combination of the improvement in hydrophilicity for membranes and the formed interconnected ions transport channels. To investigate the hydrophilicity of resulted membranes, the contact angle of substrate membrane and methanol-responsive multilayered membrane was performed as shown in Fig. 9. Methanol-responsive multilayered membrane shows a lower contact angle than that of substrate membrane due to the excellent hydrophilicity of the PE, indicating a higher hydrophilicity of methanol-responsive multilayered membranes than that of substrate membrane. On the other hand, introducing the PE layers on the inner pore wall and the surface of membrane can form the interconnected ions transport channels. These results demonstrated that the membranes with well-defined ions transport channels fabricated via the SR-LBL assembly method maintain high proton conductivity.

To further confirm the availability of this SR-LBL assembly method, EG and water, which swell lower on substrate membranes, were selected as solvents. 3 PE layers based on a PES/SPEEK porous membrane treated with different solvents were fabricated and investigated for VFB separators. As illustrated in Fig. 10, the CE of the membranes prepared from EG is 88.7%, while, the CE of 86.2% can be only obtained fabricated from water. The trend is consistent with the order of swelling of dry substrate membrane. The smaller difference in the solubility between polymers and solvents gives rise to the more swelling of membranes, which favors the deposition of the PE layers on the inner pore wall of membranes and thus results in the significantly decreased pore size of membranes. The smaller pore size of membranes can effectively separate vanadium ions and protons to improve the CE of VFB. At the same time, the VE of VFB does not greatly vary with the increasing swelling, but almost keeps constant, which indicates that the pore wall characteristics does not dramatically change with the increasing swelling. These results confirm our idea that membranes with well-defined ions transport channels could be easily fabricated via SR-LBL assembly method.

In summary, we have developed a general method for fabricating membranes with well-defined ions transport channels. The structure characterization of membranes suggests that swelling effect of solvent on membranes plays a significant role on the fabrication of solvent-responsive multilayered membranes. The excellent ions selectivity is mainly ascribed to the decreased pore size caused by the introduction of PE layers into the inner pore wall, while the high ions conductivity is mainly ascribed to the improvement in membranes hydrophilicity. As a result, the VFB single cell assembled with solvent-responsive multilayered membranes achieved an excellent battery performance at a wide current density range, thus the membranes prepared with SR-LBL can be considered very promising for VFB application. Moreover, membranes with well-defined ions transport channels fabricated using our general method can be extended to other related systems e.g. energy storage, fuel cells, and membrane separation.

Methods

Materials. Sulfonated poly (ether ether ketone) (SPEEK) was prepared by direct sulfonation of PEEK with sulfuric acid at 70°C for 2 h, as reported previously[38]. The degree of sulfonation, as obtained by ^{1}H NMR, is around 0.8[38]. Poly (ether sulfone) (PES), with viscosity of 0.58, was obtained from Changchun Jilin University Special Plastic Engineering Research. The N,N-Dimethylacetamide (DMAC), isopropyl alcohol (IPA), methanol and ethylene glycol (EG) were purchased from Tianjin Damao Chemical Reagent Factory. Poly (diallyldimethylammonium chloride) (PDDA; Mw = 200,000–350,000 g/mol) and Poly (acrylic acid) (PAA; Mw = 3,000 g/mol) were obtained from Aladdin Chemistry Co. Ltd.

Membrane matrix preparation. The PES/SPEEK NF membranes were prepared using phase inversion technique from a solution containing 28% wt PES and 7% wt SPEEK dissolved in DMAC. Then the solution was cast onto a clean glass plate at room temperature with humidity less than 40% to avoid the penetration of water vapor into the polymer solution. After evaporation for 10 s, the plate was immersed into water to form the PES/SPEEK porous membranes. The thickness of membranes was 130 ± 5 μm.

Solvent-responsive layer-by-layer assembly. PEs (PDDA and PAA) were dissolved in aqueous medium with a concentration of 2 wt%. Taking methanol as a swelling agent as an example. The PES/SPEEK porous membrane was first immersed in the methanol for 10 min to open the pores, then immersed in the solution of the cationic PE (PDDA) for 20 min and rinsed with water for 10 min. Afterward, the adsorption of the anionic PE (PAA) was similar to that of the cationic PE (PDDA) except the PE was alternated to the PAA. The described procedure was repeated to control the pore size via tuning the layer numbers (See Fig. 1b).

Scanning electronic microscopy and field emission scanning electronic microscopy (SEM and FE-SEM). The surface and cross-section morphologies of the prepared membranes were characterized by SEM (JEOL 6360LV, Japan) and FE-SEM (QUANTA 200FEG), respectively. The cross-section of membranes was obtained by breaking the membranes in liquid nitrogen. All the samples were gold coated before measurement.

Energy-dispersive X-ray spectroscopy (EDS). The weight percent of nitrogen element (N) of membranes and N distribution were obtained using EDS (MODEL QUANTA 200FEG 132-10) attached to FE-SEM.

Transmission electronic microscopy (TEM). The distribution of negatively charged groups on the cross-section of membranes was characterized by TEM (JEM-2000EX, JEOL). All the samples were stained with 0.5 M $[Pb(Ac)_2]^{2+}$ and fixed in epoxy before being cut into thin slice samples.

Attenuated total reflectance Fourier transform infrared spectroscopy (ATR-FTIR). The chemical structures of the prepared membranes were characterized by ATR-FTIR. The ATR-FTIR spectra were measured by JASCO FTIR 4100 spectrometer. Each spectrum was recorded at the average rate of 48 scans with a resolution of 4 cm^{-1} collected from 400 to 4000 cm^{-1} in reflection mode.

Atomic force microscopy (AFM). The membrane surface roughness of the prepared membranes was characterized by a Multimode AFM with a Nanoscope V controller (Veeco/Digital Instruments, Santa Barbara, USA).

Swelling measurement. Swelling of the dry membrane in various solvent was measured to correlate interaction between the membrane materials and solvents. The wet membrane was firstly dried under vacuum at 100°C for 24 h and then immersed into different solvents at room temperature for 24 h. The swelling was calculated by the following equation:

$$\text{Swelling}(\%) = \frac{L_s - L_d}{L_d} \times 100 \quad (4)$$

Where L_s is the length of the swollen membrane after treating in solvent, and L_d is the length of the dry membrane.

Contact angle. To measure the hydrophilic behavior of membrane, the contact angle of membrane was detected by using a contact angle measuring instrument (JC2001A, China). The wet membrane was firstly dried under vacuum at 50°C for 12 h. 2 μl deionized water was dropped onto dry flat membrane surface and the image was frozen after 30 seconds for each test.

Area resistance measurement. The area resistance of the membranes was measured by the method described in our previous study[39]. A conductivity cell was separated by a membrane into two compartments filled with 0.5 M H_2SO_4. The effective area of the membrane was 1 cm^2. The electric resistance was recorded by electrochemical impedance spectroscopy (EIS) over a frequency range from 1 kHz to 1 MHz. The area resistance was calculated described as follows:

$$r = (r_2 - r_1) \times s \quad (5)$$

where r_2 and r_1 were the electric resistance of the cell with and without a membrane respectively, and s is the effective area of the membrane.

All the membranes were soaked in 0.5 M H_2SO_4 for 1 day before measurement.

Average pore size distribution. Average pore size distribution of membranes was investigated via water flux measurement, which is done in a stainless steel dead-end pressure cell with 19.6 cm^2 effective membrane area. After filling the water in the cell, the device was pressurized with nitrogen and then kept at a certain pressure. Permeate samples were collected in cooled flasks as a function of time, weighed and analyzed. The average pore size of membranes was calculated by the Hagen-Poiseuille equation[40]:

$$J = \frac{\varepsilon D_2 \Delta P}{32 \eta L \tau} \quad (6)$$

Where J is the water flux, D is the average pores size, ε is the porosity, τ is the turtosity, ηis the water viscosity, L is the average thickness of membranes, ΔP is the pressure difference across the membranes.

Proton/vanadium permeability. Proton/vanadium permeability was measured by the diffusion cell as described elsewhere[8]. The left cell was filled with 1.5 M $VOSO_4$ in 3 M H_2SO_4 solution, while the right cell was filled with deionized water. Both sides were vigorously stirred to avoid concentration polarization. Samples from the right cell were collected at regular time intervals. The concentration of VO^{2+} and H^+ was characterized by a UV-vis spectrometer (JASCO, FT-IR 4100, Japan) and a Sartorious meter, respectively.

VFB single cell performance. A VFB single cell was assembled by sandwiching a membrane with two pieces of carbon felt electrodes, clamped by two pieces of polar plates. All these components were fixed between two pieces of stainless plates. The effective area of the membrane was 9 cm^2. 30 mL 1.5 M V^{2+}/V^{3+} in 3.0 M H_2SO_4 and 30 mL 1.5 M VO^{2+}/VO_2^+ in 3.0 M H_2SO_4 solutions, using as negative and positive electrolytes respectively, were cyclically pumped into the corresponding half-cell through airtight pine lines. The charge-discharge performance of the VFB was tested by Arbin BT 2000 with various current densities. The cell was charged to 1.65 V and discharged to 0.8 V for each charge-discharge cycle to avoid the corrosion of carbon felt electrodes and polar plates.

1. Dunn, B., Kamath, H. & Tarascon, J. M. Electrical Energy Storage for the Grid: A Battery of Choices. *Science* **334**, 928–935 (2011).
2. Yang, Z. G. *et al.* Electrochemical Energy Storage for Green Grid. *Chem. Rev.* **111**, 3577–3613 (2011).
3. Leadbetter, J. & Swan, L. G. Selection of battery technology to support grid-integrated renewable electricity. *J. Power Sources* **216**, 376–386 (2012).
4. Li, X. F., Zhang, H. M., Mai, Z. S., Zhang, H. Z. & Vankelecom, I. Ion exchange membranes for vanadium redox flow battery (VRB) applications. *Energ. Environ. Sci.* **4**, 1147–1160 (2011).
5. Schwenzer, B. *et al.* Membrane Development for Vanadium Redox Flow Batteries. *Chemsuschem* **4**, 1388–1406 (2011).
6. Skyllas-Kazacos, M., Chakrabarti, M. H., Hajimolana, S. A., Mjalli, F. S. & Saleem, M. Progress in Flow Battery Research and Development. *J. Electrochem. Soc.* **158**, R55–R79 (2011).
7. Skyllas-Kazacos, M., Rychcik, M., Robins, R. G., Fane, A. G. & Green, M. A. New All-Vanadium Redox Flow Cell. *J. Electrochem. Soc.* **133**, 1057–1058 (1986).
8. Zhang, H. Z., Zhang, H. M., Li, X. F., Mai, Z. S. & Zhang, J. L. Nanofiltration (NF) membranes: the next generation separators for all vanadium redox flow batteries (VRBs)? *Energ. Environ. Sci.* **4**, 1676–1679 (2011).
9. Li, Y., Zhang, H. M., Li, X. F., Zhang, H. Z. & Wei, W. P. Porous poly (ether sulfone) membranes with tunable morphology: Fabrication and their application for vanadium flow battery. *J. Power Sources* **233**, 202–208 (2013).
10. Xie, H., Saito, T. & Hickner, M. A. Zeta Potential of Ion-Conductive Membranes by Streaming Current Measurements. *Langmuir* **27**, 4721–4727 (2011).
11. Peckham, T. J. & Holdcroft, S. Structure-Morphology-Property Relationships of Non-Perfluorinated Proton-Conducting Membranes. *Adv. Mater.* **22**, 4667–4690 (2010).
12. Schoch, R. B., Han, J. Y. & Renaud, P. Transport phenomena in nanofluidics. *Rev. Mod. Phys.* **80**, 839–883 (2008).
13. Decher, G. Fuzzy nanoassemblies: Toward layered polymeric multicomposites. *Science* **277**, 1232–1237 (1997).
14. Krasemann, L., Toutianoush, A. & Tieke, B. Self-assembled polyelectrolyte multilayer membranes with highly improved pervaporation separation of ethanol/water mixtures. *J. Membrane Sci.* **181**, 221–228 (2001).
15. Seo, J., Lutkenhaus, J. L., Kim, J., Hammond, P. T. & Char, K. Development of surface morphology in multilayered films prepared by layer-by-layer deposition using poly(acrylic acid) and hydrophobically modified poly(ethylene oxide). *Macromolecules* **40**, 4028–4036 (2007).
16. Joseph, N., Ahmadiannamini, P., Hoogenboom, R. & Vankelecom, I. F. J. Layer-by-layer preparation of polyelectrolyte multilayer membranes for separation. *Polym. Chem.*, doi:10.1039/c3py01262j (2014).
17. Lee, D., Nolte, A. J., Kunz, A. L., Rubner, M. F. & Cohen, R. E. pH-induced hysteretic gating of track-etched polycarbonate membranes: Swelling/deswelling behavior of polyelectrolyte multilayers in confined geometry. *J. Am. Chem. Soc.* **128**, 8521–8529 (2006).
18. Tago, T., Shibata, H. & Nishide, H. Proton conductivity in the dry membrane of poly(sulfonic acid) and polyamine layer-by-layer complex. *Chem. Commun.*, 2989–2991 (2007).
19. Zhao, C. J., Lin, H. D., Zhang, Q. A. & Na, H. Layer-by-layer self-assembly of polyaniline on sulfonated poly(arylene ether ketone) membrane with high proton conductivity and low methanol crossover. *Int. J. Hydrogen Energ.* **35**, 10482–10488 (2010).
20. Park, J., Kwon, Y. & Lee, T. W. Layer-by-layer spin self-assembled hole injection layers containing a perfluorinated ionomer for efficient polymer light-emitting diodes. *Macromol. Rapid Comm.* **28**, 1366–1372 (2007).
21. Costa, R. R., Custodio, C. A., Arias, F. J., Rodriguez-Cabello, J. C. & Mano, J. F. Layer-by-Layer Assembly of Chitosan and Recombinant Biopolymers into Biomimetic Coatings with Multiple Stimuli-Responsive Properties. *Small* **7**, 2640–2649 (2011).
22. Pal, S. & De, G. Oriented Au-Cu nanoalloy particle incorporated SiO2 films using a new layer by layer deposition technique. *J. Mater. Chem.* **17**, 493–498 (2007).
23. Shon, Y. S. *et al.* Stability and Morphology of Gold Nanoisland Arrays Generated from Layer-by-Layer Assembled Nanoparticle Multilayer Films: Effects of Heating Temperature and Particle Size. *J. Phys. Chem. C* **115**, 10597–10605 (2011).
24. Charinpanitkul, T. *et al.* Improved hydrophilicity of zinc oxide-incorporated layer-by-layer polyelectrolyte film fabricated by dip coating method. *J. Ind. Eng. Chem.* **18**, 1441–1445 (2012).
25. Dey, P., Linnanen, L. & Pal, P. Separation of lactic acid from fermentation broth by cross flow nanofiltration: Membrane characterization and transport modelling. *Desalination* **288**, 47–57 (2012).
26. Ma, J. & Zhou, L. L. A new procedure for calculating Hansen solubility parameters of carbon nanotube/polymer composites. *Polym. Bull.* **68**, 1053–1063 (2012).
27. Denisyuk, E. Y. Swelling in the Mechanically Loaded Polymer Networks. *Polym. Sci. Ser. a+* **52**, 436–446 (2010).
28. Hansen, C. M. & Smith, A. L. Using Hansen solubility parameters to correlate solubility of C-60 fullerene in organic solvents and in polymers. *Carbon* **42**, 1591–1597 (2004).
29. Redelius, P. Bitumen solubility model using Hansen solubility parameter. *Energ. Fuel* **18**, 1087–1092 (2004).
30. Evans, K. M. & Hardy, J. K. Predicting solubility and permeation properties of organic solvents in viton glove material using Hansen's solubility parameters. *J. Appl. Polym. Sci.* **93**, 2688–2698 (2004).
31. Li, X. F. *et al.* Solvent-resistant nanofiltration membranes based on multilayered polyelectrolyte complexes. *Chem. Mater.* **20**, 3876–3883 (2008).
32. Zhang, H. Z., Zhang, H. M., Li, X. F., Mai, Z. S. & Wei, W. P. Silica modified nanofiltration membranes with improved selectivity for redox flow battery application. *Energ. Environ. Sci.* **5**, 6299–6303 (2012).

33. Wei, W. P. *et al.* Hydrophobic asymmetric ultrafiltration PVDF membranes: an alternative separator for VFB with excellent stability. *Phys. Chem. Chem. Phys.* **15**, 1766–1771, doi:10.1039/C2cp43761a (2013).
34. Barton, A. F. M. *CRC handbook of solubility parameters and other cohesion parameters*. 2nd edn, (CRC Press, 1991).
35. Dubas, S. T. & Schlenoff, J. B. Factors controlling the growth of polyelectrolyte multilayers. *Macromolecules* **32**, 8153–8160 (1999).
36. Oriji, G., Katayama, Y. & Miura, T. Investigations on V(IV)/V(V) and V(II)/V(III) redox reactions by various electrochemical methods. *J. Power Sources* **139**, 321–324 (2005).
37. Tuckerman, M., Laasonen, K., Sprik, M. & Parrinello, M. Ab-Initio Molecular-Dynamics Simulation of the Solvation and Transport of H3o+ and Oh- Ions in Water. *J. Phys. Chem-Us* **99**, 5749–5752 (1995).
38. Xing, P. X. *et al.* Synthesis and characterization of sulfonated poly(ether ether ketone) for proton exchange membranes. *J. Membrane Sci.* **229**, 95–106 (2004).
39. Mai, Z. S., Zhang, H. M., Li, X. F., Bi, C. & Dai, H. Sulfonated poly(tetramethydiphenyl ether ether ketone) membranes for vanadium redox flow battery application. *J. Power Sources* **196**, 482–487 (2011).
40. Li, W. X., Xing, W. H. & Xu, N. P. Modeling of relationship between water permeability and microstructure parameters of ceramic membranes. *Desalination* **192**, 340–345 (2006).

Acknowledgments

The authors greatly acknowledge the financial support from National Basic Research Program of China (973 program No. 2010CB227202), and China Natural Science Foundation (No. 21206158).

Author contributions

W.X. performed the experiments, analyzed the data, and wrote the initial manuscript draft. X.L. and H.M.Z. designed and oversaw the experiments, revised and finalized the manuscript for submission. J.C. and H.Z.Z. participated in project planning and discussions of the results. All authors reviewed the manuscript.

Additional information

Supplementary information accompanies this paper at http://www.nature.com/scientificreports

Competing financial interests: The authors declare no competing financial interests.

How to cite this article: Xu, W., Li, X.F., Cao, J.Y., Zhang, H.Z. & Zhang, H.M. Membranes with well-defined ions transport channels fabricated via solvent-responsive layer-by-layer assembly method for vanadium flow battery. *Sci. Rep.* **4**, 4016; DOI:10.1038/srep04016 (2014).